Water Research 230 (2023) 119592

Contents lists available at ScienceDirect

Water Research

journal homepage: www.elsevier.com/locate/watres

Mercury migration to surface water from remediated mine waste and impacts of rainfall in a karst area – Evidence from Hg isotopes

Junyao Yan [a,b], Ruolan Li [a,b], Muhammad Ubaid Ali [a], Chuan Wang [a,b], Bo Wang [a], Xingang Jin [a], Mingyu Shao [a,b], Ping Li [a,*], Leiming Zhang [c], Xinbin Feng [a]

[a] State Key Laboratory of Environmental Geochemistry, Institute of Geochemistry, Chinese Academy of Sciences, Guiyang, China
[b] University of Chinese Academy of Sciences, Beijing, China
[c] Air Quality Research Division, Science and Technology Branch, Environment and Climate Change Canada, Toronto M3H 5T4, Canada

ARTICLE INFO

Keywords:
Mercury
Mine waste
Remediation
Rainfall
Mercury isotope
Karst area

ABSTRACT

Mine waste (MW) in historical mercury (Hg) mining areas continuously emits Hg into local environment, including aquatic ecosystems. Tracing Hg migration process from MW and determining its relative contribution to Hg pollution is critical for understanding the environmental impact of MW remediation. In this study, we combined data of Hg concentration, speciation, and isotope to address this issue in the Wanshan Hg mining area in southwest China. We found that rainfall can elevate Hg concentrations in river water and control the partitioning and transport of Hg in karst fissure zones through changing the hydrological conditions. A consistently large offset of δ^{202}Hg (1.24‰) was observed between dissolved Hg (DHg) and particulate Hg (PHg) in surface water during the low-flow period (LFP), which may have been related to the relatively stable hydrologic conditions and unique geological background (karst fissure zones) of the karst region (KR). Results from the ternary Hg isotopic mixing model showed that, despite an order of magnitude reduction in Hg concentration and flux in river water after remediation, the remediated MW is still a significant source of Hg pollution to local aquatic ecosystems, accounting for 49.3 ± 11.9% and 37.8 ± 11.8% of river DHg in high flow period (HFP) and LFP, respectively. This study provides new insights into Hg migration and transportation in aquatic ecosystem and pollution source apportionment in Hg polluted area, which can be used for making polices for future remediation actions.

1. Introduction

Mercury (Hg) is a toxic pollutant and is listed as a priority pollutant by many international agencies (Jiang et al., 2006; Kwon et al., 2020). Mining activities, such as gold and Hg mining, have increased the Hg concentration by three-fold in surface water compared to pre-anthropogenic condition (Amos et al., 2013; Lamborg et al., 2014; Streets et al., 2011). The Wanshan Hg mine (WMM), which is known as the "capital of Hg", is located in a karst region (KR) in southwest China. Although Hg mining activities were banned in 2001, long-term mining activities have caused severe Hg pollution in local ecosystems (Feng et al., 2008; Horvat et al., 2003; Li et al., 2008; Qiu et al., 2013; Kim et al., 2016; Xia et al., 2020). Mine waste (MW) is the product of high-temperature ore roasting, and it contains large amounts of secondary soluble Hg. The total mercury (THg) and methylmercury (MeHg) levels in the surface water flowing through the MW were significantly elevated compared to that of the background area (Zhang et al., 2010a, 2010b). In addition, the KR of southwest China is one of the largest karst geomorphologic distributing areas in the world (Huang et al., 2008). KR showed high Hg background and unique aquifers plays a unique role in the global Hg biogeochemical cycle (Xia et al., 2022).

Erosion is a major factor in watersheds with significant MW storage during rainfall-runoff events (especially stormwater). This process can lead to serious Hg emission and diffusion, increasing the environmental risks to local aquatic ecosystems (Guedron et al., 2011; Rose et al., 2012; Zheng et al., 2016). In the KR, large inter-annual variations and differences between pre- and after-rainfall events in Hg emissions have created a regime of hydrologic extremities. However, the role of rainfall in the release of Hg from MW and subsequent transfer to aquatic systems remains unclear.

The "Action Plan for Soil Pollution Prevention and Control" was implemented in China in 2016. Typical restoration measures such as

* Corresponding author.
E-mail address: liping@mail.gyig.ac.cn (P. Li).

https://doi.org/10.1016/j.watres.2023.119592
Received 8 November 2022; Received in revised form 4 January 2023; Accepted 6 January 2023
Available online 8 January 2023

capping with sand or clay were implemented in this area, and these methods were considered as economical and effective remediation approaches to control pollution in aquatic ecosystems. However, sand and clay have a relatively weak affinity for Hg and cannot prevent Hg migration through the cap via the pore water pathway (Eckley et al., 2020). Furthermore, enhanced flux of Hg to surface water has been demonstrated by mesocosm experiments because of the low organic carbon content of sand caps (Curtis et al., 2019). Evaluating the effects of restoration treatments requires quantification of Hg emission flux to downstream water bodies, which is a challenging but crucial for projecting future changes at Hg contaminated sites.

Because of the difficulties in determining the water flow through MW, traditional methods cannot be used to calculate Hg emission flux from MW based on surface water Hg concentration. Stable Hg isotopes are represented by a three-dimensional system that may not be affected by uncertain factors, such as the Hg concentration and stream discharge. The unique Hg isotopic composition of various reservoirs in Hg mining areas could be used to effectively tracing the migration pathways and sources of Hg in fluvial systems (Blum et al., 2014; Delphine et al., 2009; Yin et al., 2010a). Because of extremely low concentration of Hg in surface water, Hg in water must be extracted and pre-concentrated for Hg isotopic analysis.

Mass-dependent fractionation (MDF) occurs in almost all environmental processes such as adsorption and desorption (Jiskra et al., 2012), diffusion (Koster van Groos et al., 2014), evaporation (Zheng et al., 2019), microbial methylation and demethylation (Janssen et al., 2016;

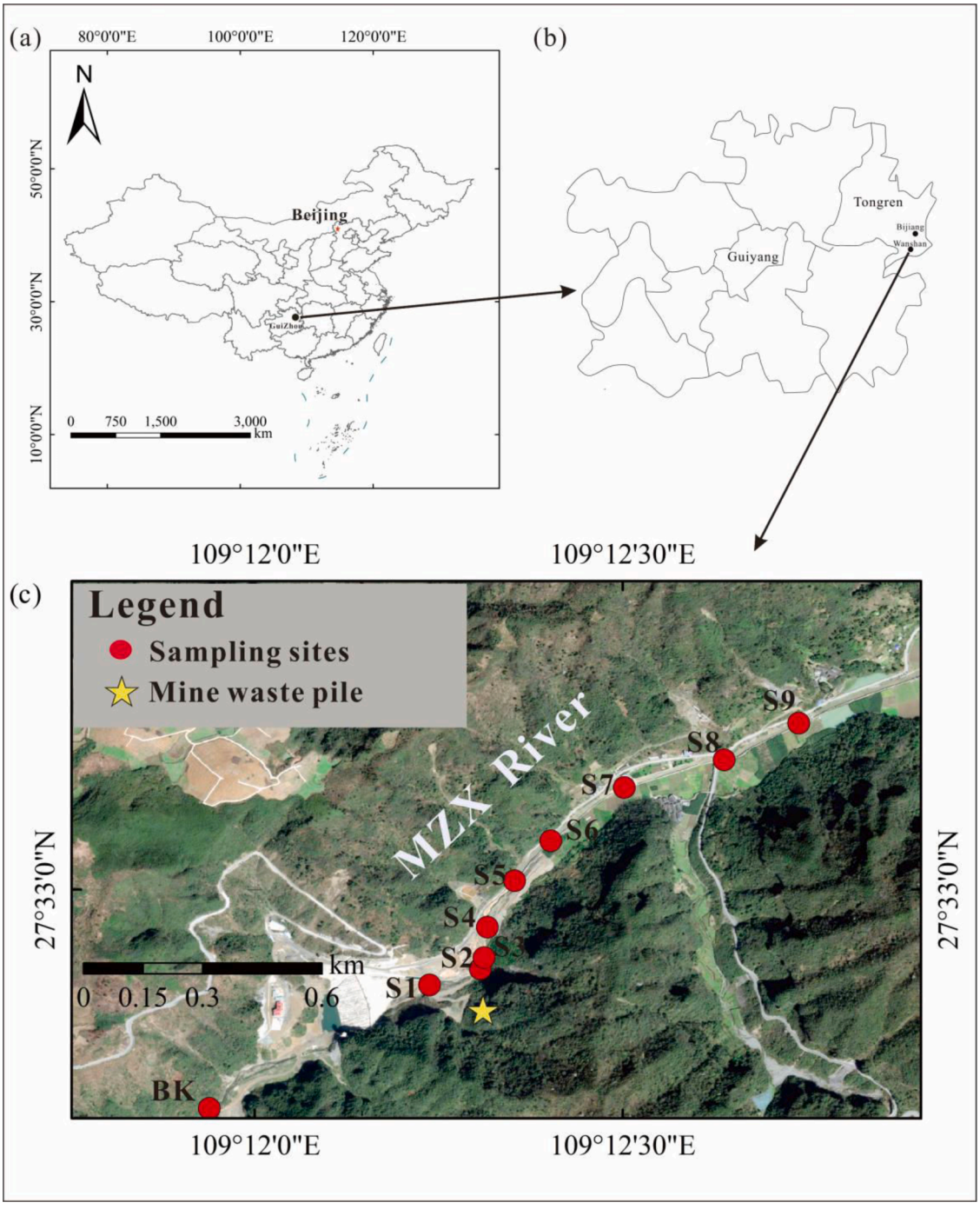

Fig. 1. Spatial distribution of sampling sites in MZX river.

Kritee et al., 2009), and Hg uptake by plants (Yin et al., 2013a; Yuan et al., 2019). Mass-independent fractionation (MIF) is caused by the magnetic isotope effect and nuclear volume effect (Bergquist and Blum 2007; Estrade et al., 2009), and MIE in photochemical reactions are the main reasons for global MIF (Biswas et al., 2008; Buchachenko 2001; Carignan et al., 2009; Chen et al., 2012; Sonke 2011; Sun et al., 2014; Zheng et al., 2007). To utilize Hg isotopes as a tracer for Hg cycling and pollution sources, the fractionation factors for important biogeochemical processes must be determined (Smith et al., 2015). Prior studies have demonstrated that MDF may occur during transformation of cinnabar to by-products due to the roasting process, because calcines (−0.08±0.20‰) were enriched by 0.8‰ in δ^{202}Hg values compared to the unroasted Hg ores (−0.74±0.11‰) in the WMM (Yin et al., 2013b). Delphine et al. (2009) found that the Hg isotopic composition of cinnabar was similar to that of the river sediment, and presumed that the sediments throughout the watershed of the Isonzo River to the Gulf of Trieste were seriously impacted by Hg export from the Idrija Hg mine. Previous studies mainly focused on smelter-affected sediments or agricultural regains (Feng et al., 2010; Lepak et al., 2020; Song et al., 2021; Washburn et al., 2017) and identified Hg pollution sources. However, the migration process and transport mechanism of Hg from pollution sources to fluvial systems remain to be unclear.

The objectives of this study were to 1) assess the Hg flux from remediated MWs and evaluate the remediation effect; 2) clarify the role of rainfall in Hg release from the MW; and 3) quantify the contribution of Hg emission from the MW using the Hg stable isotope approach. Findings from this study are expected to reveal the role of the MWs in the regional Hg cycle and provide scientific basis and data support for the formulation of remediation policies for Hg-contaminated solid waste.

2. Materials and methods

2.1. Study area

The Wanshan Hg mine is located in Wanshan County of Guizhou Province, within the karst landscape of the Yunnan-Guizhou Plateau (Fig. 1a and b). The study area has a sub-tropical climate with humid condition and an annual precipitation of 1110–1410 mm. In this study, a typical remediated MW pile, named Meizixi (MZX), was chosen because it is located in a typical karst area and its headwaters were stacked with remediation MW (Fig. 1c). It is situated upstream of and connects to several small and shallow streams with numerous downstream tributaries. Its aquifers are characterized with high spatial heterogeneity and complex subterranean conduit networks.

2.2. Sample collection

To effectively evaluate the contributions of Hg emission from MW to MZX, we focused on the upstream source of this river and a reach of it within a 2 km radius. Water samples were collected from the river near MW pile, natural springs, and precipitation during normal flow periods (NFPs) (October 2020), low flow periods (LFPs) (December 2020), and high flow periods (HFP) (July 2021). In the HFP, surface water samples were collected at the same point before and after the rainfall event. Before sampling, three ultrapure water samples were prepared in the laboratory as field blanks.

Within a vertical MW profile, a thin steel rod was driven horizontally into the profile to avoid obstacles, and provide a clear pilot channel for a 10 cm porous polymer tube (Eijkelkamp Agrisearch Equipment, Netherlands). The solution was left for two weeks to equilibrate with the soil, and 10 mL of pore water was extracted using a vacuum tube (Moreno-Jimenez et al., 2011).

All water samples were collected in duplicate. Unfiltered river water samples were collected for THg and total methylmercury (TMeHg) analyses. The surface water samples were filtered in situ using a 0.45 μm polyvinylidene fluoride filter (Millipore) for dissolved Hg (DHg) and dissolved methyl Hg (DMeHg) analyses. The water samples were stored in 200 mL borosilicate bottles, which were decontaminated using acidic solution, followed by rinsing with deionized water and incineration for 1.5 h in a muffle furnace at 480 °C. After filtration, the water samples were acidified with ultra-pure hydrochloric acid, sealed, packaged in double-layer bags, returned to the laboratory and stored in a refrigerator at 4 °C. At each sampling site, 1 L of water was collected and filtered using a Teflon filter membrane to determine the total suspended solids (TSS). The TSS value was used to calculate the distribution coefficients (log(Kd)) using the DHg concentration of the filtered surface water and suspended material, following the method described by James et al. (1998).

The water flow (Q) was measured by cup-type current meter (LS45A). The basic physical and chemical parameters of the surface water were measured in situ during the sampling process. Water temperature (WT), pH, electrical conductivity (EC, 25 °C), and dissolved oxygen (DO) were measured using a portable PONSEL ODEON meter, which was calibrated prior to deployment using pH (4, 7, and 10), EC (1412 μS/cm), and DO (0% and 100%) standards. The measurement accuracies of the device for the pH, WT, DO, and EC were 0.01, 0.01 °C, 1%, and 0.01 μS/cm, respectively.

2.3. Sample preparation for Hg isotope analysis

Filtered surface water and suspended particle samples for Hg isotope analysis were collected during LFP and HFP. To ensure the minimum Hg concentration required for the Hg isotope analysis, each filtered surface water sample was pre-enriched based on the method established by Li et al. (2019). Approximately 2–5 L water samples were used to determine the Hg isotopes. The samples were acidified successively using 0.5% (v: v) ultrapure hydrochloric acid in the field and then transported back to the laboratory for cold storage. Before enrichment, a 0.5% BrCl solution was added for oxidation for at least 48 h. The oxidized water samples were transferred to a bubble bottle. A small amount of $NH_2OH{\cdot}HCl$ solution was added to remove excess BrCl. Then, a 0.5% $SnCl_2$ solution was added to reduce Hg^{2+} to Hg^0, which was purged with 2.5 L/min of zero Hg gas for 1 h, and the evaporated Hg was pre-concentrated into a chlorinated activated carbon tube. The Hg captured by chlorinated activated carbon was removed by the pyrolysis device and absorbed into 5 mL of 40% anti-aqua regia (v:v, HNO_3: HCl = 2:1). The solutions were stored in a refrigerator at 4 °C away from light before Hg isotope analysis (Li et al., 2019).

For PHg, a high temperature purified Teflon membrane was used to filter an appropriate amount of water (2–5 L), and the filter membranes were freeze-dried and digested at high temperature using a tubular muffle furnace to extract Hg into a 5 mL of a 40% anti aqua regia absorption liquid (Fu et al., 2013).

2.4. Hg concentration and Hg isotope analysis

The operationally defined fractions of THg, PHg, and DHg in the surface water samples were determined using a dual stage Au amalgamation method and cold vapor atomic fluorescence spectrophotometer (CVAFS). DHg and THg were determined following BrCl oxidation for 24 h and then reduced to Hg^0 using acidic $SnCl_2$. PHg was obtained by subtracting DHg from THg. The TMeHg and DMeHg concentrations were determined by distillation, ethylation, GC separation, and CVAFS (Guo et al., 2008; Jiang et al., 2004).

The isotopic composition of Hg was analyzed using MC-ICPMS (Nu Instruments, UK). The measurement procedures were described in detail by Yin et al. (2010b). Thallium internal corrections, external standards, and sample bracketing method were used to obtain precise and accurate measurements. An internal Tl standard (NIST 997) was introduced to correct instrumental mass bias. Strict sample-standard bracketing with a solution of NIST 3133 that was matched in terms of the concentration and solution matrix was used for mass bias correction. MDF was

expressed in delta notation (δ) relative to NIST 3133, and it was calculated using Eq. (1).

$$\delta^{xxx}Hg_{sample}(\%) = \left[\left({}^{xxx/198}Hg_{sample}/{}^{xxx/198}Hg_{NIST3133} - 1\right)\right] \times 1000 \quad (1)$$

where xxx represents 199, 200, 201, 202, or 204. MIF is reported as the deviation from the theoretically predicted δ^{xxx}Hg values based on the kinetic mass fractionation law and is reported with capital delta notation (Δ^{xxx}Hg), which is calculated using Eqs. (2) - (5), respectively.

$$\Delta^{199}Hg = \delta^{199}Hg - \delta^{202}Hg \times 0.252 \quad (2)$$

$$\Delta^{200}Hg = \delta^{200}Hg - \delta^{202}Hg \times 0.502 \quad (3)$$

$$\Delta^{201}Hg = \delta^{201}Hg - \delta^{202}Hg \times 0.752 \quad (4)$$

$$\Delta^{204}Hg = \delta^{204}Hg - \delta^{202}Hg \times 1.493 \quad (5)$$

The fractions of Hg in the water filtered through MW (WTM), which are derived from MW, open precipitation (OP), and background water (BW), were calculated using a triple-member mixing model as follows:

$$\delta^{202}Hg_{WTM} = \delta^{202}Hg_{BW} \times f_{BW} + \delta^{202}Hg_{OP} \times f_{OP} + \delta^{202}Hg_{MW} \times f_{MW} \quad (6)$$

$$\Delta^{199}Hg_{WTM} = \Delta^{199}Hg_{BW} \times f_{BW} + \Delta^{199}Hg_{OP} \times f_{OP} + \Delta^{199}Hg_{MW} \times f_{MW} \quad (7)$$

$$f_{BW} + f_{OP} + f_{MW} = 1 \quad (8)$$

where f_{BW}, f_{OP}, and f_{MW} are the fraction ratios of the BW, OP, and MW respectively. Based on Eqs. (6)–(8), random number generation was performed in RStudio (Windows) and then the Monte Carlo simulation method (n = 10,000) was used to estimate the relative contributions of the three end-members. The uncertainties in the triple mixing model were also estimated using the Monte Carlo simulation approach.

2.5. Quality control

The quality assurance and quality control of the Hg analysis were assessed using blanks, blind duplicates, and matrix spikes. The recoveries for the matrix spikes averaged at 101%±4% for THg and 81% ±16% for MeHg. The relative standard deviation was ≤8% for the Hg concentration analysis. The recovery rates of the enrichment test of the water samples ranged from 95% to 110%. The results of the UM-Almadén standard solution (δ^{202}Hg: −0.59‰±0.06‰; Δ^{199}Hg: 0.03‰ ±0.04‰; Δ^{201}Hg: 0.01‰±0.05‰, 2σ, n = 8) and GSS-4 standard for sediment (δ^{202}Hg: −1.85‰±0.02‰; Δ^{199}Hg: −0.43‰±0.02‰; Δ^{201}Hg: −0.36‰±0.04‰, 2σ, n = 3) were consistent with those reported in previous studies (Blum and Bergquist 2007; Estrade et al., 2010).

2.6. Data analysis

The data were analyzed using SPSS 26.0 and Origin 2018 software. The characteristics of THg and other Hg forms in the water samples were reported as the mean±standard deviation (SD) and examined using descriptive statistics. A nonparametric test was used to compare the differences between different data groups. Correlation and difference tests were considered to be statistically significant at $p < 0.05$.

3. Results and discussion

3.1. Temporal variation of water Hg and Hg emission flux

THg and DHg concentrations during the HFP (32.6 ± 16.3 ng/L and 23.6 ± 12.2 ng/L, respectively) were significantly higher than those during the LFP (14.8 ± 9.8 ng/L and 7.4 ± 4.1 ng/L, respectively) (p<0.05), whereas PHg concentrations were not significantly different between these two periods (9.0 ± 6.4 versus 7.8 ± 8.8 ng/L, p>0.05) (Fig. S1 and Table S1). The concentrations of TMeHg in HFP were slightly higher than those in the other two periods (ANOVA, p>0.05). The average TMeHg concentrations are given in the Section S2. Both water discharge and hydrodynamic conditions governed Hg concentration. In the HFP, stronger hydrodynamic conditions, higher flows, and enhanced erosion led to Hg transport from the MW into the river, resulting in significantly higher THg and DHg concentrations compared with the case of LFP. Meanwhile, a significant dilution effect on PHg was observed during the HFP. In contrast, relatively weak hydrodynamic conditions might have resulted in the deposition of PHg at the riverbed. Rainfall has a combined effect of erosion and leaching on the MW, thus leading to Hg dissolution in MW and then releasing into rivers (Gray et al., 2003; Kim et al., 2000). The solidified MW pile is more stable and leaching effect is dominated compared with erosion, so DHg was the dominant form compared with PHg. However, no significant seasonal differences in PHg were observed. The highest THg, DHg, and PHg concentrations were observed near the MW pile during the HFP, indicating that MW is an important source of Hg to downstream regions due to erosion and leaching during rainfall.

Note that MW pile at MZX was sprayed with a passivator and covered with soil in 2013, and then vegetation was planted above the pile. Besides, the surrounding river channel was also dredged. To evaluate the effectiveness of these restoration actions, we compared our data collected in 2020–2021 with those reported before 2013 (Qiu et al., 2005; Zhang et al., 2010a, 2010b). Only data from sampling locations close to the MW pile (within 1.5 km) were selected for accurate comparison (Fig. 2). Because the historical flow of this stretch of the river could not be determined, the arithmetic averages of Hg concentration were used for comparison.

Most DHg and PHg concentrations observed in the present study were lower than level I of the national standard for surface water (50 ng/L) except at some points near MW during HFP. THg and DHg concentrations during NFP (20.7 ± 14.8 ng/L and 7.25±4.30 ng/L, respectively) and THg and PHg concentrations during HFP were significantly lower in 2020 than 2002 (p<0.05). Overall decreasing trends from 2008 to 2020 were observed in the different forms of Hg (THg, DHg, and PHg), despite of insignificant differences between the two years (Fig. 2). The maximum THg concentration (69 ng/L; near the MW) observed in this study was reduced by an order of magnitude compared to that observed at the MZX River in 2011 (316 ng/L) (Dai, 2011). The average water flows of the MZX River at the MW cross-section were 0.119 m^3/s, 0.075 m^3/s, and 0.187 m^3/s and the corresponding Hg fluxes were 32.9 ± 23.6 g/y, 5.7 ± 3.5 g/y, and 47.4 ± 23.8 g/y during the NFP, LFP, and HFP, respectively (the calculation methods are shown in Section S1.1). Therefore, the THg emission flux from the MZX pile to the river was estimated be 109.7 ± 50.9 g/y. Compared with the Hg flux calculated by Dai (2011) for this section of the river (1480 g/y), the Hg flux in this study also decreased by an order of magnitude.

The above results illustrate the significant effect of the remediation arrangement. However, THg concentration in this study was still slightly higher than the background surface water values, indicating MW piles being still a major source of Hg pollution in local aquatic ecosystems in Hg mining areas (Yan et al., 2019). MW contains large amounts of secondary compounds of Hg produced under high-temperature conditions, which are released continuously to the surrounding environment by rainfall leaching, runoff, and volatilization. Therefore, the proportional contribution of Hg emission from MW to surface water needs to be further elucidated, particularly in relation to erosion and leaching induced by rainfall.

3.2. Effects of rainfall

The MZX River is mainly fed by spring water and rainfall. To further clarify the impact of rainfall on surface water Hg concentrations, we collected data of a rainfall event in the HFP. The velocity of water flow at the cross section of MW pile increased significantly from 0.08 m^3/s to

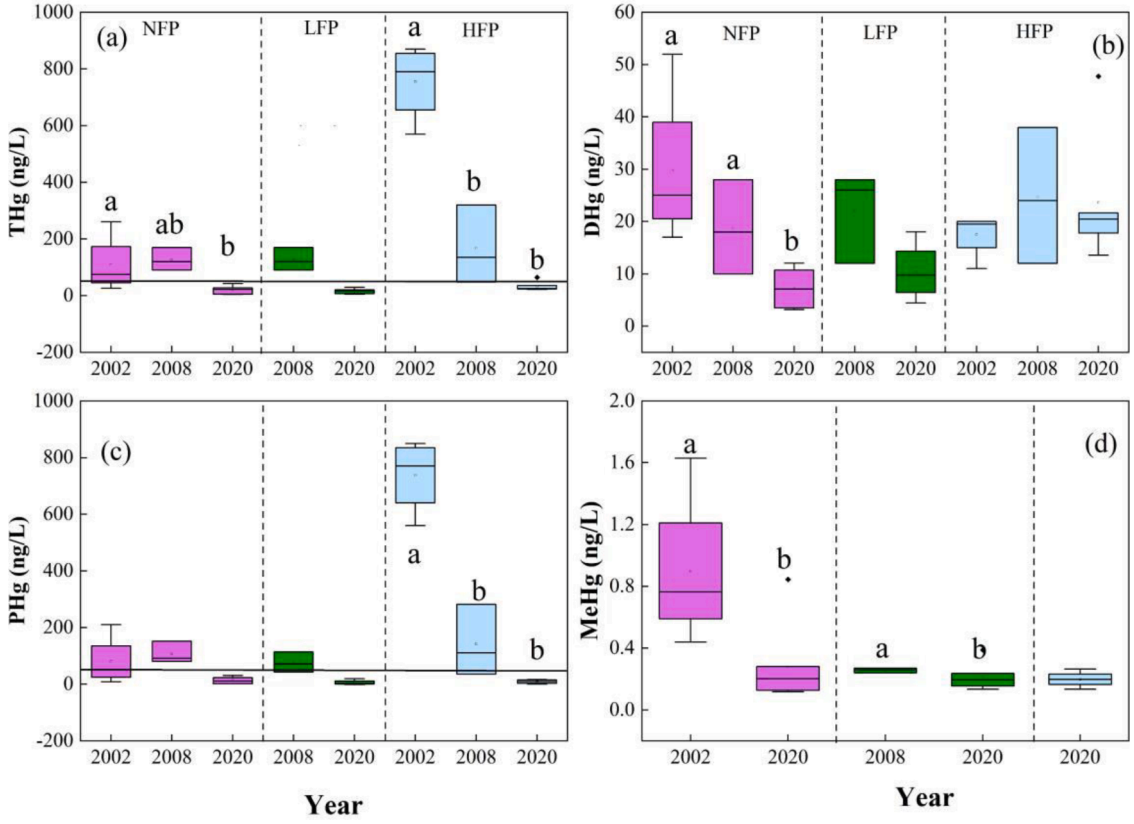

Fig. 2. Temporal variation of speciation Hg concentration in MZX. Solid line represents the US limit value (50 ng/L) for fresh water (USEPA, 1999) (The Hg concentration in 2002 and 2008 were adopted from Qiu et al. (2005) and Zhang et al. (2010a, 2010b), respectively.). Each box represents an the 25th and 75th percentile interquartile ranges, the band near the middle of the box is the 50th percentile (median), and the whiskers represent the 5th and 95th percentiles.

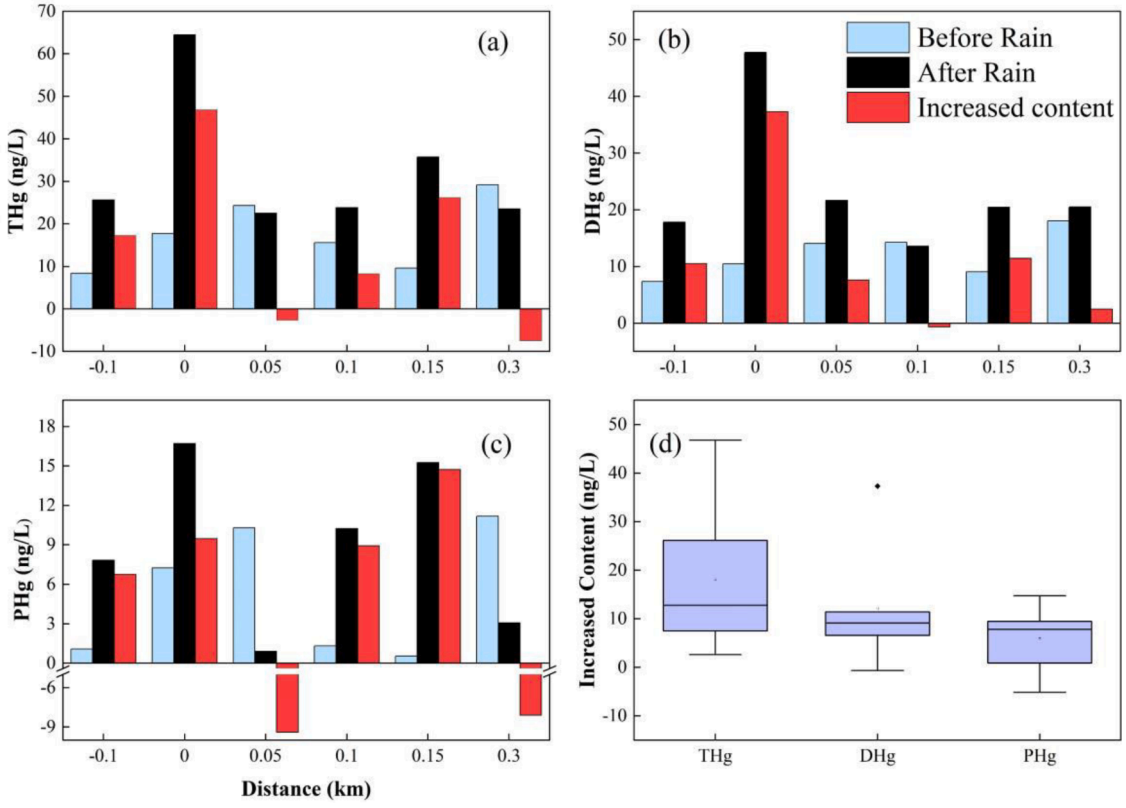

Fig. 3. Hg concentration variations in surface water before and after the rainfall event.

0.19 m^3/s pre- and after the rainfall event. In addition, the THg, DHg, and PHg concentrations in the surface water increased by 15.2 ± 19.5 ng/L, 11.4 ± 13.5 ng/L, and 3.7 ± 10.0 ng/L, respectively, due to the initial erosion effect (Fig. 3). The much higher increment in DHg than PHg concentration is consistent with their variation trends in the surface water between the HFP and LFP (Fig. S1).

The pH and conductivity in surface water should respond rapidly to a rainfall event, therefore, these parameters were used below as indicators to explore the influence of rainfall on Hg concentrations in surface water. The average pH and conductivity in the rainwater were 6.8 ± 0.3 and 33.9 ± 19.9 μs/cm, respectively; and those in the surface water were 8.5 ± 0.1 and 287.8 ± 24.2 μs/cm, respectively, before the rainfall, and 7.9 ± 0.1 and 359.8 ± 5.6 μs/cm after the rainfall event (Fig. S2a and S2b). At the KR, rainfall dilution and water-rock-gas interactions are the two main controlling factors on the hydrochemical indices of surface water. The lower pH and conductivity in rainwater than surface water and the significantly increased conductivity in the surface water after the rainfall event indicated that the direct contribution of rainfall to surface water conductivity was small. However, it is very likely that rainfall indirectly affected surface water through increasing the erosion and leaching of Hg from the surrounding MWs, which led to increases in water conductivity, as previously reported by Liu et al. (2007). More discussions on this mechanism are presented below.

3.3. Hg isotopes in DHg and PHg

In the LFP, the δ^{202}Hg values of DHg and PHg in surface water near the MW pile averaged at −0.56±0.13‰ and 0.61±0.33‰, respectively (Fig. 4 and Table S2). Compared with those of the MW (0.09±0.23‰), the δ^{202}Hg values of PHg in surface water were more positive (Fig. 5) because lighter Hg can be more easily dissolved from MW. A consistent offset of δ^{202}Hg values (1.24‰±0.22‰) was observed between DHg and PHg regardless of whether flow through the MW pile occurred or not, and this value was statistically significant ($p<0.01$, $n = 9$). Washburn et al. (2017) also found similar results in the South River (0.28‰), which is a gravel-bed river located in a valley in the USA; however, the offset of δ^{202}Hg was far less than that of our study. In addition, the South River aquatic ecosystems are dominated by PHg, which has low solubility and is relatively unreactive, leading a slight variation in its isotopic composition (Schudel et al., 2018). Smith et al. (2015) found enrichments of light Hg isotopes in the precipitated β-HgS relative to the dissolved Hg in the laboratory with acid condition (pH=2.3), and the offset of δ^{202}Hg was −0.63‰, while the dissolution process in our study caused positive offset in weak alkaline conditions (pH=8.2 ± 0.3). The DHg concentrations from the source of MZX to the MW pile averaged at 8.4 ± 7.6 ng/L and 23.6 ± 12.2 ng/L while those of the PHg concentrations averaged at 3.0 ± 4.5 ng/L and 9.0 ± 6.4 ng/L during the LFP and HFP, respectively. The proportion of DHg to THg was relatively high during the LFP and HFP, with averages of 88.9% and 73.4%, respectively. However, Washburn et al. (2017) indicated that the average proportion of DHg to THg was 23.9% in the hyporheic zones of the channel margins of the South River. To eliminate interference during the sampling process and more effectively describe the partitioning of DHg and PHg in fluvial systems, the distribution coefficient (Kd) was adopted in this study based on the method of James et al. (1998) (see the method details in Section S1.2). The log (Kd) values arithmetically averaged at 5.0 ± 0.8 and 5.8 ± 0.5 in the LFP and HFP, respectively. These values were much lower than those observed at the South River (6.0–6.5), indicating a greater predominance of DHg in our study.

The DHg in this study is functionally defined as Hg that passed through a 0.45 μm filter, and it may be related to colloidal dissolved organic matter (DOM), which contains a variety of ligands with affinities for Hg. When Hg enters the water column due to erosion and leaching, a portion of Hg is quickly adsorbed by sulfhydryl groups with high affinity that are present in DOM (Wiederhold et al., 2010). When the adsorption reaches saturation, larger suspended particles with weak affinity to Hg will also adsorb a part of Hg (Hesterberg et al., 2001; Hintelmann and Harris 2004; Skyllberg et al., 2006). Multiple studies have shown that the binding effect of Hg to DOM (low Hg/DOM ratio) is controlled by a small fraction of DOM molecules that contain a reactive thiol functional group under natural conditions (Haitzer et al., 2002). In addition, Hg isotope fractionation in the HgS system was likely dominated by ligand exchange in solution from Hg-O to Hg-S coordination (Smith et al., 2015), and thiol-bound Hg was enriched in light Hg isotopes by 0.53‰ and 0.62‰ (δ^{202}Hg) relative to $HgCl_2$ and $Hg(OH)_2$, respectively (Wiederhold et al., 2010). The mechanism in the hyporheic zone is complicated and requires further investigation.

We speculate that the different geological backgrounds and types of Hg-contaminated sites are also responsible for the large differences in the offsets. The strata of the South River area are dominated by sandstone (Jaillard et al., 1999), while that in the present study have a unique karst geological background. Moreover, the capacity to store and transmit water in KR varies widely owing to the complex structure and degree of karstification because of the extensive network of interconnected joints, fractures, and dissolution cavities. The water column of the KR was characterized by high pH and low turbidity. The South

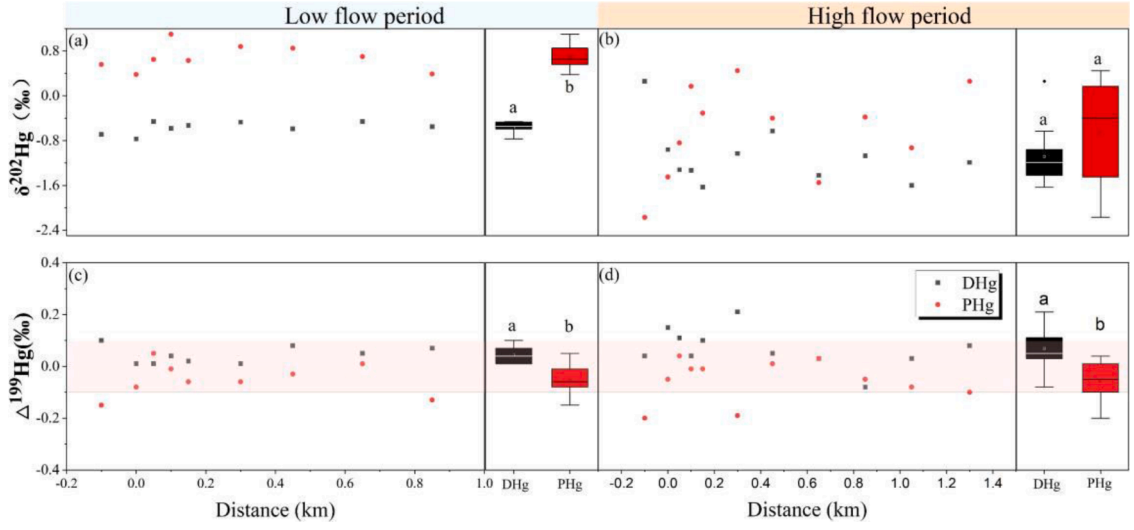

Fig. 4. Hg isotopic compositions of DHg and PHg in surface water around the mine waste pile. Sampling locations are presented in relative river kilometers. The measured error bars represent ±2 standard deviations.

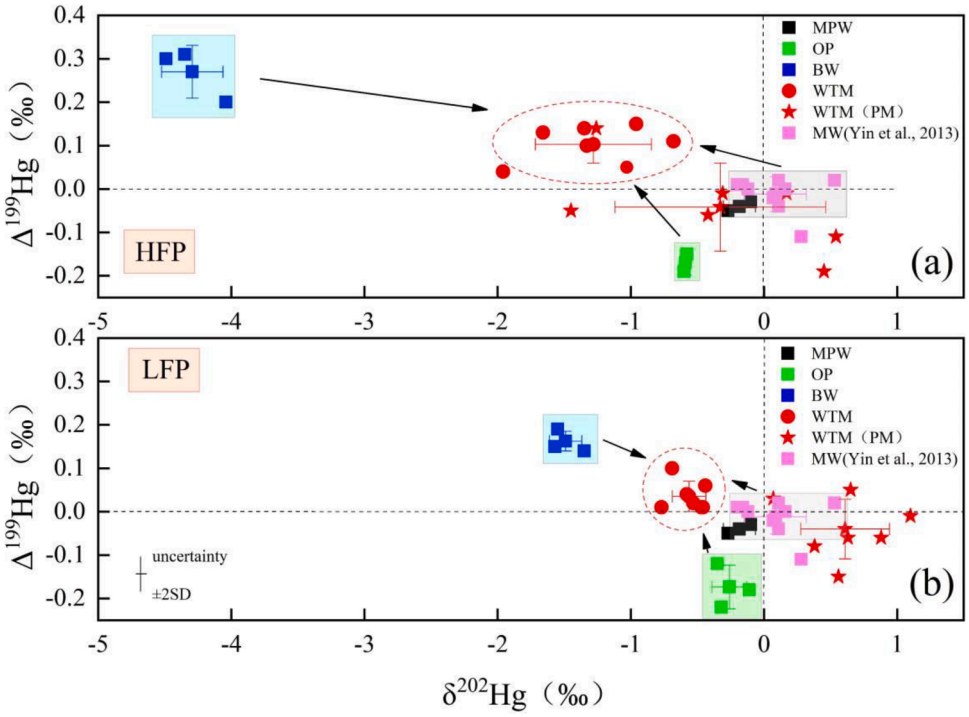

Fig. 5. Three end-member isotopic mixing models for DHg were presented as δ^{202}Hg vs. Δ^{199}Hg (‰) values.

River was polluted by a chemical plant used to recover elemental Hg from sludge, however, our study was conducted at a Hg mining area in a low temperature metallogenic zone. Thus, the Hg species and isotopic compositions varied significantly between the two studies. Compared to the δ^{202}Hg values of PHg in the South River (−0.68‰), the apparently positive δ^{202}Hg values found in the present study (0.61±0.33‰) are also responsible for the large offset of δ^{202}Hg between PHg and DHg. Moreover, the δ^{202}Hg values of the pore water in the channel margin hyporheic zone (δ^{202}Hg=−0.52±0.44‰) were significantly higher than those of the surface waters (δ^{202}Hg=−0.89±0.20‰) (Washburn et al., 2018). Furthermore, the resuspension of sediments from the river bed into the water column may reduce the overall Hg isotopic fractionation in the South River. However, in the present study, remediation was carried out in the river channel, and the riverbed was filled with gravel without sediment.

The δ^{202}Hg values of DHg and PHg averaged at −1.26±0.41‰ and −0.53±0.69‰, respectively, during the HFP. Compared with the case during the LFP, the δ^{202}Hg values during the HFP were generally negative and varied greatly, and a relatively stable offset was not observed. This conclusion is consistent with that for the South River mentioned above, likely due to the influence of hydrologic conditions on water Hg partitioning and Hg isotope fractionation (Washburn et al., 2018). After a certain period of time, adsorption/dissolution equilibrium is attained because of the weaker hydrodynamic condition in the LFP. The Hg isotopic values of the MW were located between PHg and DHg, indicating sufficient water-rock dissolution and limited exogenous input. However, the hydrologic conditions in the hyporheic zone changed significantly because of the plentiful rainfall in the HFP, especially in the KR; thus, the isotopic compositions of PHg in WTM were close to those of the MW (Fig. 5). The Δ^{199}Hg values of DHg and PHg were close to 0, regardless of the hydrological seasonality (Section S3), and all surface water samples showed a Δ^{199}Hg/Δ^{201}Hg ratio of 1 in both LFP (Fig. S3) and HFP (Fig. S4).

3.4. Source identification by Hg isotopes

In the surface water near the MW, DHg was the predominant form; thus, we used Δ^{199}Hg and δ^{202}Hg to quantify the relative contribution of Hg pollution from MW, OP, and BW to the surface water Hg Eqs. (6)–((8)). Here, upstream surface water with a low-Hg concentration that did not flow through the MW is defined as the BW. THg concentrations were significantly elevated when water flowed through the MW and then gradually decreased downstream, which is similar to the findings of previous studies (Dai et al., 2013; Qiu et al., 2009; Zhang et al., 2010a). The Hg isotopic values of pore water of MW (MPW) are mixtures of MW and OP, and only a slightly negative offset was observed between MPW and MW, which may be caused by OP. Based on this hypothesis, MW was directly regarded as an end-member. To eliminate the influence of other sources, only sampling points near the MW and before passing through the farmland were considered in this study. Because of the short distance between sampling sites (within 1 km), we assumed that it is only a rapid mixing process when different end-members enter the receiving water, and significant MDF and MIF will not occur during this rapid mixing process.

The average THg concentrations in BW, OP, and WTM were 12.2 ng/L, 201 ng/L, and 15.5 ng/L, respectively, during LFP, and were 6.8 ng/L, 327.8 ng/L, and 69.0 ng/L during HFP (summer time). Note that the average THg concentration in the MPW was 181 ng/L (Section S4). The THg concentrations were negatively correlated with the Δ^{199}Hg values (Fig. 6). Higher THg concentrations were observed in WTM, and the Δ^{199}Hg values were close to the MPW and OP signals (Fig. 6). In addition, the differences in the δ^{202}Hg values between the three sources were significant ($p<0.05$), thus allowing for the development of a constrained Hg isotopic mixing model with good confidence. In this study, we used the δ^{202}Hg and Δ^{199}Hg values for source tracing, and their relationship is presented in Fig. 5. The data points were interpreted as the result of triple mixing of the three end-members. BW was characterized by a slightly positive Δ^{199}Hg and negative δ^{202}Hg, and OP was characterized by a negative Δ^{199}Hg.

Based on the Δ^{199}Hg-δ^{202}Hg mixing model, the direct contribution of OP to DHg was relatively small at 13.2 ± 9.28% and 15.8 ± 10.6% in the HFP and LFP, respectively. We found that the contribution of OP to DHg in surface water was mainly associated with the erosion and leaching of MW and bedrock (as mentioned in Section 3.2). Although rainfall

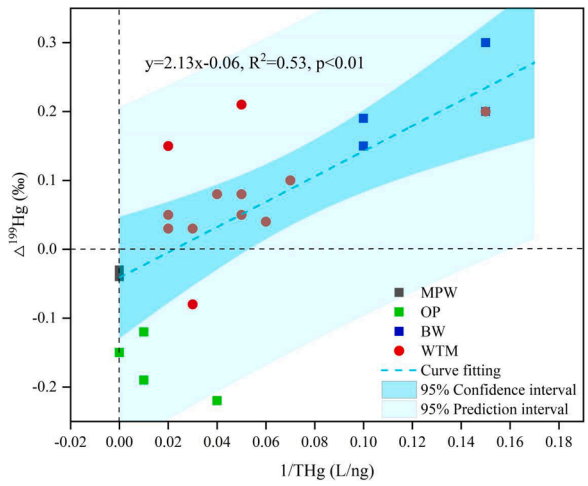

Fig. 6. Plot of Δ^{199}Hg (‰) vs 1/THg (L/ng) in MPW, OP, BW and WTM.

amounts varied greatly between the HFP and LFP, the contributions of OP to DHg in WTM were similar between these two periods. In the Hg mining area, atmospheric Hg from the local sources enters the water column through wet deposition because PHg is the main Hg form in OP. The isotopic values of PHg in OP were very close to those in WTM during the HFP (Fig. S5a), but were different from those in WTM during the LFP (Fig. S5b), indicating that rainfall mainly contributed to PHg in the surface water (Section S4).

The contributions of MW (f_{MW}) to DHg in WTM were 49.3 ± 11.9% and 37.8 ± 11.8%, and those of BW were 37.5 ± 6.48% and 46.4 ± 7.15% in the HFP and LFP, respectively. Thus, MW is still a major source of DHg in the mining-affected surface water. Rainfall is abundant in the HFP, and the erosion and leaching effects are significant; therefore, contributions of rainfall to surface water Hg were significant in the HFP. Despite of low discharge of rainwater flowing through MW in the LFP, the contribution of MW to surface water Hg could still reach 37.8% owing to the relatively high Hg concentrations in the flow. The contributions of BW to surface water Hg were comparable to those of MW, mainly due to the two contrasting factors, i.e. relatively high discharge and relatively low Hg concentration. As the main Hg form in surface water, DHg is characterized by a strong migration ability, which may pose great environmental risks to downstream aquatic ecosystems. In this study, we firstly combined the Δ^{199}Hg and δ^{202}Hg signals to quantify the rainfall-induced DHg pollution from MW to surface water and highlighted the need for further integrated monitoring of the source and quantity of DHg downstream.

4. Conclusions and implications

This study found significantly higher surface water Hg concentrations during HFP than LFP and very different surface water Hg concentrations between the periods pre- and after-rainfall events. These results suggest that erosion and leaching of MW and bedrock into the water column may be the main factors underlying the above phenomena. It is also found that rainfall-induced variability in hydrologic conditions in karst fissure pipes may affect the Hg isotopic partitioning between DHg and PHg in surface waters.

During the LFP, sufficient dissolution equilibrium may have occurred because of the stable hydrologic conditions; therefore, a consistent offset of δ^{202}Hg (1.24‰) was observed between DHg and PHg. In addition, this offset was much higher than that reported in previous studies, which was likely due to the unique geological background of the KR with high pH, low turbidity, and relatively low DOM. Overall, the precipitation and dissolution processes may lead to the consistent fractionation between DHg and PHg. Hydrodynamic conditions alter the degree of water-rock interaction and thus determine the degree of fractionation. The temporal variations of Hg concentration and mixing model results indicated that remediation work can reduce the Hg concentration and flux from MW to surface water. However, the remediated MW pile remains a source of Hg for the local aquatic environment.

The consistent offset of δ^{202}Hg between PHg and DHg in surface water provides a fundamental framework for understanding of Hg isotope fractionation during mineral dissolution in natural water. It indicates that Hg isotopes are a powerful indicator of Hg migration and transportation in aquatic ecosystem and pollution source apportionment in Hg polluted areas. Results from the present study provide an important scientific basis for developing economical and practical remediation policies for Hg-containing solid waste.

Declaration of Competing Interest

The authors declare that they have no known competing financial interests or personal relationships that could have appeared to influence the work reported in this study.

Data availability

Data will be made available on request.

Acknowledgments

This study was funded by the Strategic Priority Research Program of Chinese Academy of Sciences (XDB40020400), National Natural Science Foundation of China (41921004, U1612442), the Central Government Leading Local Science and Technology Development (QianKeZhongYinDi [2021]4028), Guizhou Provincial Science and Technology Subsidies, the CAS Interdisciplinary Innovation Team (JCTD-2020–20), and Youth Innovation Promotion Association of Chinese Academy of Sciences (Y2021106).

Supplementary materials

Supplementary material associated with this article can be found, in the online version, at doi:10.1016/j.watres.2023.119592.

References

Amos, H.M., Jacob, D.J., Streets, D.G., Sunderland, E.M., 2013. Legacy impacts of all-time anthropogenic emissions on the global mercury cycle. Glob. Biogeochem. Cycles 27 (2), 410–421.
Bergquist, B.A., Blum, J.D., 2007. Mass-dependent and -independent fractionation of hgisotopes by photoreduction in aquatic systems. Science 318, 417–420.
Biswas, A., Blum, J.D., Bergquist, B.A., Keeler, G.J., Xie, Z., 2008. Natural Mercury isotope variation in coal deposits and organic soils. Environ. Sci. Technol. 42, 8303–8309.
Blum, J.D., Bergquist, B.A., 2007. Reporting of variations in the natural isotopic composition of mercury. Anal. Bioanal. Chem. 388, 353–359.
Blum, J.D., Sherman, L.S., Johnson, M.W., 2014. Mercury isotopes in earth and environmental sciences. Annu. Rev. Earth Planet. Sci. 42 (1), 249–269.
Buchachenko, A.L., 2001. Buchachenko magnetic isotope effect nuclear spin control of chemical reactions. J. Phys. Chem. 105, 44.
Carignan, J., Estrade, N., Sonke, J.E., Donard, O.F.X., 2009. Odd isotope deficits in atmospheric Hg measured in lichens. Environ. Sci. Technol. 43, 5660–5664.
Chen, J., Hintelmann, H., Feng, X., Dimock, B., 2012. Unusual fractionation of both odd and even mercury isotopes in precipitation from Peterborough, ON, Canada. Geochim. Cosmochim. Acta 90, 33–46.
Curtis, A.N., Bourne, K., Borsuk, M.E., Buckman, K.L., Demidenko, E., Taylor, V.F., Chen, C.Y., 2019. Effects of temperature, salinity, and sediment organic carbon on methylmercury bioaccumulation in an estuarine amphipod. Sci. Total Environ. 687, 907–916.
Dai, Z., 2011. Mass Balance of Mercury in a Catchment of Wanshan Hg Mining Area. Guizhou Province.
Dai, Z., Feng, X., Zhang, C., Shang, L., Qiu, G., 2013. Assessment of mercury erosion by surface water in Wanshan mercury mining area. Environ. Res. 125, 2–11.
Delphine, F., Nives, O., Holger, H., 2009. Tracing mercury contamination from the Idrija mining region (Slovenia) to the Gulf of Trieste using Hg isotope ratio measurements. Environ. Sci. Technol. 43, 33–39.

Eckley, C.S., Gilmour, C.C., Janssen, S., Luxton, T.P., Randall, P.M., Whalin, L., Austin, C., 2020. The assessment and remediation of mercury contaminated sites: a review of current approaches. Sci. Total Environ. 707, 136031.
Estrade, N., Carignan, J., Sonke, J.E., Donard, O.F.X., 2009. Mercury isotope fractionation during liquid–vapor evaporation experiments. Geochim. Cosmochim. Acta 73 (10), 2693–2711.
Estrade, N., Carignan, J., Sonke, J.E., Donard, O.F.X., 2010. Measuring Hg isotopes in bio-Geo-environmental reference materials. Geostand. Geoanal. Res. 34, 79–93.
Feng, X., Foucher, D., Hintelmann, H., Yan, H., He, T., Qiu, G., 2010. Tracing mercury contamination sources in sediments using mercury isotope compositions. Environ. Sci. Technol. 44, 3363–3368.
Feng, X., Li, P., Qiu, G., Wang, S., Li, G., Shang, L., Meng, B., Jiang, H., Bai, W., Li, Z., Fu, X., 2008. Human exposure to methylmercury through rice intake in mercury mining areas, Guizhou province, China. Environ. Sci. Technol. 42, 326–332.
Fu, X., Feng, X., Yin, R., Zhang, H., 2013. Diurnal variations of total mercury, reactive mercury, and dissolved gaseous mercury concentrations and water/air mercury flux in warm and cold seasons from freshwaters of southwestern China. Environ. Toxicol. Chem. 32 (10), 2256–2265.
Gray, J.E., Greaves, I.A., Bustos, D.M., Krabbenhoft, D.P., 2003. Mercury and methylmercury contents in mine-waste calcine, water, and sediment collected from the Palawan Quicksilver Mine, Philippines. Environ. Geol. 43 (3), 298–307.
Guedron, S., Grimaldi, M., Grimaldi, C., Cossa, D., Tisserand, D., Charlet, L., 2011. Amazonian former gold mined soils as a source of methylmercury: evidence from a small scale watershed in French Guiana. Water Res. 45 (8), 2659–2669.
Guo, Y., Feng, X., Li, Z., He, T., Yan, H., Meng, B., Zhang, J., Qiu, G., 2008. Distribution and wet deposition fluxes of total and methyl mercury in Wujiang River Basin, Guizhou, China. Atmos. Environ. 42 (30), 7096–7103.
Haitzer, M., Aiken, G.R., Ryan, J.N., 2002. Binding of Mercury(II) to dissolved organic matter the role of the mercury-to-DOM concentration ratio. Environ. Sci. Technol. 36, 3564–3570.
Hesterberg, D., Chou, J., Hutchison, K., Saters, D., 2001. Bonding of Hg(II) to reduced organic sulfur in humic acid as affected by S/Hg ratio. Environ. Sci. Technol. 35, 2741–2745.
Hintelmann, H., Harris, R., 2004. Application of multiple stable mercury isotopes to determine the adsorption and desorption dynamics of Hg(II) and MeHg to sediments. Mar. Chem. 90 (1–4), 165–173.
Horvat, M., Nolde, N., Fajon, V., Jereb, V., Logar, M., Lojen, S., Jacimovic, R., Falnoga, I., Liya, Q., Faganeli, J., Drobne, D., 2003. Total mercury, methylmercury and selenium in mercury polluted areas in the province Guizhou, China. Sci. Total Environ. 304 (1–3), 231–256.
Huang, Q.H., Cai, Y.L., Xing, X.S., 2008. Rocky desertification, antidesertification, and sustainable development in the karst mountain region of Southwest China. Ambio A J. Hum. Environ. 37 (5), 390–392.
Jaillard, E., Laubacher, G.r., Bengtson, P., Dhondt, A.V., Bulote, L.G., 1999. Stratigraphy and evolution of the Cretaceous forearc Celica-Lancones basin of southwestern Ecuador. J. South Am. Earth Sci. 12, 51–68.
James, P.H., Susan, E.C., Martin, M.S., Peter, E.H., 1998. Partitioning and transport of total and methyl mercury in the lower fox river, Wisconsin. Environ. Sci. Technol. 32, 1424–1432.
Janssen, S.E., Schaefer, J.K., Barkay, T., Reinfelder, J.R., 2016. Fractionation of mercury stable isotopes during microbial methylmercury production by iron- and sulfate-reducing bacteria. Environ. Sci. Technol. 50 (15), 8077–8083.
Jiang, G., Shi, J., Feng, X., 2006. Mercury pollution in China. Environ. Sci. Technol. 3673–3678.
Jiang, H., Feng, X., Liang, L., Shang, L., Yan, H., Chou, Y., 2004. Determination of methyl mercury in waters by distillation-GC-CVAFS technique. China Environ. Sci. 24, 568–571.
Jiskra, M., Wiederhold, J.G., Bourdon, B., Kretzschmar, R., 2012. Solution speciation controls mercury isotope fractionation of Hg(II) sorption to goethite. Environ. Sci. Technol. 46 (12), 6654–6662.
Kim, C.S., Brown, G.E., Rytuba, J.J., 2000. Characterization and speciation of mercury-bearing mine wastes using X-ray absorption spectroscopy. Sci. Total Environ. 261, 157–168.
Kim, K.H., Kabir, E., Jahan, S.A., 2016. A review on the distribution of Hg in the environment and its human health impacts. J. Hazard. Mater. 306, 376–385.
Koster van Groos, P.G., Esser, B.K., Williams, R.W., Hunt, J.R., 2014. Isotope effect of mercury diffusion in air. Environ. Sci. Technol. 48, 227–233.
Kritee, K., Barkay, T., Blum, J.D., 2009. Mass dependent stable isotope fractionation of mercury during mer mediated microbial degradation of monomethylmercury. Geochim. Cosmochim. Acta 73 (5), 1285–1296.
Kwon, S.Y., Blum, J.D., Yin, R., Tsui, M.T.-K., Yang, Y.H., Choi, J.W., 2020. Mercury stable isotopes for monitoring the effectiveness of the Minamata Convention on Mercury. Earth Sci. Rev. 203, 103111.
Lamborg, C.H., Hammerschmidt, C.R., Bowman, K.L., Swarr, G.J., Munson, K.M., Ohnemus, D.C., Lam, P.J., Heimbürger, L.E., Rijkenberg, M.J.A., Saito, M.A., 2014. A global ocean inventory of anthropogenic mercury based on water column measurements. Nature 512 (7512), 65–68.
Lepak, R.F., Janssen, S.E., Engstrom, D.R., Krabbenhoft, D.P., Tate, M.T., Yin, R., Fitzgerald, W.F., Nagorski, S.A., Hurley, J.P., 2020. Resolving atmospheric mercury loading and source trends from isotopic records of remote North American lake sediments. Environ. Sci. Technol. 54 (15), 9325–9333.
Li, K., Lin, C.J., Yuan, W., Sun, G., Fu, X., Feng, X., 2019. An improved method for recovering and preconcentrating mercury in natural water samples for stable isotope analysis. J. Anal. At. Spectrom. 34 (11), 2303–2313.
Li, P., Feng, X., Shang, L., Qiu, G., Meng, B., Liang, P., Zhang, H., 2008. Mercury pollution from artisanal mercury mining in Tongren, Guizhou, China. Appl. Geochem. 23 (8), 2055–2064.
Liu, Z., Li, Q., Sun, H., Wang, J., 2007. Seasonal, diurnal and storm-scale hydrochemical variations of typical epikarst springs in subtropical karst areas of SW China: soil CO_2 and dilution effects. J. Hydrol. (Amst) 337 (1–2), 207–223.
Moreno-Jimenez, E., Beesley, L., Lepp, N.W., Dickinson, N.M., Hartley, W., Clemente, R., 2011. Field sampling of soil pore water to evaluate trace element mobility and associated environmental risk. Environ. Pollut. 159 (10), 3078–3085.
Qiu, G., Feng, X., Wang, S., Fu, X., Shang, L., 2009. Mercury distribution and speciation in water and fish from abandoned Hg mines in Wanshan, Guizhou province, China. Sci. Total Environ. 407 (18), 5162–5168.
Qiu, G., Feng, X., Wang, S., Shang, L., 2005. Mercury and methylmercury in riparian soil, sediments, mine-waste calcines, and moss from abandoned Hg mines in east Guizhou province, southwestern China. Appl. Geochem. 20 (3), 627–638.
Qiu, G., Feng, X., Meng, B., Zhang, C., Gu, C., Du, B., Lin, Y., 2013. Environmental geochemistry of an abandoned mercury mine in Yanwuping, Guizhou Province, China. Environ. Res. 125, 124–130.
Rose, N.L., Yang, H., Turner, S.D., Simpson, G.L., 2012. An assessment of the mechanisms for the transfer of lead and mercury from atmospherically contaminated organic soils to lake sediments with particular reference to Scotland, UK. Geochim. et Cosmochim. Acta 82, 113–135.
Schudel, G., Miserendino, R.A., Veiga, M.M., Velasquez-Lopez, P.C., Lees, P.S.J., Winland-Gaetz, S., Davee Guimaraes, J.R., Bergquist, B.A., 2018. An investigation of mercury sources in the Puyango-Tumbes River: using stable Hg isotopes to characterize transboundary Hg pollution. Chemosphere 202, 777–787.
Skyllberg, U., Bloom, P.R., Jin, Q., Lin, C., William, F.B., 2006. Complexation of mercury (II) in soil organic matter: EXAFS evidence for linear two-coordination with reduced sulfur groups. Environ. Sci. Technol. 40, 4174–4180.
Smith, R.S., Wiederhold, J.G., Kretzschmar, R., 2015. Mercury isotope fractionation during precipitation of metacinnabar (beta-HgS) and montroydite (HgO). Environ. Sci. Technol. 49 (7), 4325–4334.
Song, Z., Wang, C., Ding, L., Chen, M., Hu, Y., Li, P., Zhang, L., Feng, X., 2021. Soil mercury pollution caused by typical anthropogenic sources in China: evidence from stable mercury isotope measurement and receptor model analysis. J. Clean. Prod. 288, 125687.
Sonke, J.E., 2011. A global model of mass independent mercury stable isotope fractionation. Geochim. Cosmochim. Acta 75 (16), 4577–4590.
Streets, D.G., Devane, M.K., Lu, Z., Bond, T.C., Sunderland, E.M., Jacob, D.J., 2011. All-time releases of mercury to the atmosphere from human activities. Environ. Sci. Technol. 45 (24), 10485–10491.
Sun, R., Sonke, J.E., Heimburger, L.E., Belkin, H.E., Liu, G., Shome, D., Cukrowska, E., Liousse, C., Pokrovsky, O.S., Streets, D.G., 2014. Mercury stable isotope signatures of world coal deposits and historical coal combustion emissions. Environ. Sci. Technol. 48 (13), 7660–7668.
USEPA, 1999. Recommended Water Quality Criteria – Correction. US Environmental Protection Agency, Office of Water. 822-Z-99-001.
Washburn, S.J., Blum, J.D., Demers, J.D., Kurz, A.Y., Landis, R.C., 2017. Isotopic characterization of mercury downstream of historic industrial contamination in the South River, Virginia. Environ. Sci. Technol. 51 (19), 10965–10973.
Washburn, S.J., Blum, J.D., Kurz, A.Y., Pizzuto, J.E., 2018. Spatial and temporal variation in the isotopic composition of mercury in the South River, VA. Chem. Geol. 494, 96–108.
Wiederhold, J.G., Cramer, C.J., Daniel, K., Infante, I., Bourdon, B., Kretzschmar, R., 2010. Equilibrium mercury isotope fractionation between dissolved Hg species and thiol-bound Hg. Environ. Sci. Technol. 44, 4191–4197.
Xia, J., Wang, J., Zhang, L., Anderson, C.W.N., Wang, X., Zhang, H., Dai, Z., Feng, X., 2020. Screening of native low mercury accumulation crops in a mercury-polluted mining region: agricultural planning to manage mercury risk in farming communities. J. Clean. Prod. 262, 121324.
Xia, J., Wang, J., Zhang, L., Wang, X., Yuan, W., Peng, T., Zheng, L., Tian, W., Feng, X., 2022. Migration and transformation of soil mercury in a karst region of southwest China: implications for groundwater contamination. Water Res. 226, 119271.
Yan, J., Wang, C., Wang, Z., Yang, S., Li, P., 2019. Mercury concentration and speciation in mine wastes in Tongren mercury mining area, southwest China and environmental effects. Appl. Geochem. 106, 112–119.
Yin, R., Feng, X., Meng, B., 2013a. Stable mercury isotope variation in rice plants (Oryza sativa L.) from the Wanshan mercury mining district, SW China. Environ. Sci. Technol. 47 (5), 2238–2245.
Yin, R., Feng, X., Shi, W., 2010a. Application of the stable-isotope system to the study of sources and fate of Hg in the environment: a review. Appl. Geochem. 25 (10), 1467–1477.
Yin, R., Feng, X., Wang, J., Li, P., Liu, J., Zhang, Y., Chen, J., Zheng, L., Hu, T., 2013b. Mercury speciation and mercury isotope fractionation during ore roasting process and their implication to source identification of downstream sediment in the Wanshan mercury mining area, SW China. Chem. Geol. 336, 72–79.
Yin, R.S., Feng, X.B., Foucher, D., Shi, W.F., Zhao, Z.Q., Wang, J., 2010b. High precision determination of mercury isotope ratios using online mercury vapor generation system coupled with multicollector inductively coupled plasma-mass spectrometer. Chin. J. Anal. Chem. 38 (7), 929–934.
Yuan, W., Sommar, J., Lin, C.J., Wang, X., Li, K., Liu, Y., Zhang, H., Lu, Z., Wu, C., Feng, X., 2019. Stable isotope evidence shows *re*-emission of elemental mercury vapor occurring after reductive loss from foliage. Environ. Sci. Technol. 53 (2), 651–660.
Zhang, H., Feng, X., Larssen, T., Shang, L., Vogt, R.D., Lin, Y., Li, P., Zhang, H., 2010a. Fractionation, distribution and transport of mercury in rivers and tributaries around

Wanshan Hg mining district, Guizhou Province, Southwestern China: part 2 – Methylmercury. Appl. Geochem. 25 (5), 642–649.
Zhang, H., Feng, X., Larssen, T., Shang, L., Vogt, R.D., Rothenberg, S.E., Li, P., Zhang, H., Lin, Y., 2010b. Fractionation, distribution and transport of mercury in rivers and tributaries around Wanshan Hg mining district, Guizhou province, southwestern China: part 1 – Total mercury. Appl. Geochem. 25 (5), 633–641.
Zheng, W., Demers, J.D., Lu, X., Bergquist, B.A., Anbar, A.D., Blum, J.D., Gu, B., 2019. Mercury stable isotope fractionation during abiotic dark oxidation in the presence of thiols and natural organic matter. Environ. Sci. Technol. 53 (4), 1853–1862.
Zheng, W., Foucher, D., Hintelmann, H., 2007. Mercury isotope fractionation during volatilization of Hg(0) from solution into the gas phase. J. Anal. At. Spectrom. 22, 1097–1104.
Zheng, Y., Luo, X., Zhang, W., Wu, X., Zhang, J., Han, F., 2016. Transport mechanisms of soil-bound mercury in the erosion process during rainfall-runoff events. Environ. Pollut. 215, 10–17.